Periodic oscillations for a graphene-based electrostatic micro actuator

Daniel Elias Nuñez (denunez@javerianacali.edu.co)
Pontificia Universidad Javeriana https://orcid.org/0000-0003-1921-8184
Larry Murcia
Pontificia Universidad Javeriana
Jorge Galan
University of Seville: Universidad de Sevilla

Research Article

Keywords: Graphene, MEMS, periodic solutions, stability, Lower and Upper Solutions Method

Posted Date: July 29th, 2021

DOI: https://doi.org/10.21203/rs.3.rs-738867/v1

Nonlinear Dynamics manuscript No.
(will be inserted by the editor)

Periodic oscillations for a graphene-based electrostatic micro actuator

Daniel E. Núñez · Jorge Galán-Vioque · Larry Murcia

Received: date / Accepted: date

Abstract We study the mechanical oscillations for a novel model of a graphene-based electrostatic parallel plates micro actuator introduced by Wei et al.(2017), considering damping effects when a periodic voltage with alternating current is applied. Our analysis starts from recent results about this MEMS model with constant voltage, and provides new insights on the periodic mechanical responses for a variable input voltage. We derive sufficient conditions on the system physical components for which periodic oscillations with constant sign exist together with their stability properties. Specifically, under some conditions, the existence of three periodic solutions is established, one of them is negative and the others are positive in sign. The positive one nearby the origin is asymptotically locally stable, whilst the other two are unstable. Additionally, we prove that no further constant sign periodic solutions can be found. The existence of periodic solutions is approached from direct and reverse order Lower and Upper Solutions Method, and the stability assertions are derived from the Liapounoff-Zukovskii criteria for Hill's equations and the linearization principle. Theoretical results are complemented by numerical simulations and numerical continuation results. Furthermore, these numerical simulations evidence the robustness of the graphene-based MEMS model over the traditional ones.

Keywords Graphene · MEMS · periodic solutions · stability · Lower and Upper Solutions Method

Mathematics Subject Classification (2020) 34D20 · 37G15 · 37N20 · 70K40

Daniel E. Núñez
Departamento de Ciencias Naturales y Matemáticas. Pontificia Universidad Javeriana Cali, Facultad de Ingeniería y Ciencias, 760031, Cali, Colombia
E-mail: denunez@javerianacali.edu.co
Corresponding author

Jorge Galán-Vioque
Instituto de Matemáticas de la Universidad de Sevilla and Departamento de Matemática Aplicada II, Escuela Técnica Superior de Ingeniería, Universidad de Sevilla, Sevilla, España
E-mail: jgv@us.es

Larry Murcia
Departamento de Ciencias Naturales y Matemáticas. Pontificia Universidad Javeriana Cali, Facultad de Ingeniería y Ciencias, 760031, Cali, Colombia
E-mail: larry061198@javerianacali.edu.co

1 Introduction

The acronym MEMS stands for microelectromechanical systems, which could be defined ac-

cording to [22,5] as the integration of mechanical elements, sensors, actuators, and electronics components on a common material substrate (typically silicon) through micro fabrication technology (micro-parts), and as a whole system. These micro-scale devices can be used as physical quantities sensors (e.g., inertia, pressure, mass, temperature, force and humidity sensors) and as actuators (e.g., RF switches, micro-grippers and thermal actuators). These micro-systems have opened the gates to a lot of possibilities, since they provide high performance, long-life and smart functionalities, and the achievement of complicated tasks in small places, everything by low fabrication and operational costs (even with zero operational cost for self-powered devices which harvest the necessary energy from the environment [22]). It is important to notice that, although Silicon is the preferred material to fabrication of MEMS due to its excellent thermal and mechanical properties [22], there are some novel materials like graphene that provide an outperformance. Next we briefly review some properties of the graphene.

The graphene can be defined as an allotrope of carbon (see [9]), which can be understood at a first sight as a monolayer of carbon atoms that are tightly bounded, and organized into a 2D mesh like a planar honeycomb lattice [13]. This novel material has astonishing properties mainly due to its sigma bonding; therefore, graphene can be even 100 times stronger than steel (see [12]) and it can have exceptional friction, elastic and thermal behavior that makes it suitable for applications in electronic devices.

In [6] the authors present a novel graphene-polyaniline nanocomposite material, which used in supercapacitors could surpass traditional ones with applications in high powered portable devices. A review of some electrical and mechanical properties, and some synthesis processes of graphene and carbon nanotubes focusing on applications in sensors and actuators can be found in [23]. For more applications see [9,13, 20,24,15,11].

On the other hand, as mentioned in [22] researchers on MEMS are usually leaded to perform several experimental tests by a trial-and-error approach, which carries longer design times and higher costs. Thus, in order to reduce them, we need a more theoretical approach based on mathematical modeling and simulating, allowing the design of higher quality devices (with novel materials) and optimize the performance of those available. For that purpose one of most popular modeling strategies consists in the treatment of the system like a lumped spring-mass one. Thus in this paper we focus on the mechanical response of electrostatic MEMS based on graphene, and specifically their oscillations due to a periodic input voltage through a nonlinear differential equation of this kind inspired by [21] .

From a mathematical point of view there are some recent results about the qualitative behavior of the oscillations for these kind of electrostatic actuated MEMS, when considering constant or periodic input voltage. Perhaps the first paper in this line using an analytical approach is due to Pelesko in [1]. Later in [7] the authors study existence and stability of periodic solutions for a canonical MEMS model called the Nathanson's model with constant or T-periodic input voltage, using classical topological techniques, and obtaining the existence of a saddle-node bifurcation for T-periodic solutions.

In [14], some sufficient conditions for existence and stability properties of periodic solutions for two periodically forced canonical MEMS models: the Nathanson's model and the Comb-drive finger model (see [22] chapter 3.5.1 and 3.5.3 respectively) are provided using Averaging Theory and Lower and Upper Solutions Method.

In [16] the authors consider the Nathanson's model and the Comb-drive finger model with cubic stiffness and without damping, and obtain existence, multiplicity and linear stability results for positive periodic solutions. A new stability phenomenon is underlying in the Comb-drive model for large cubic stiffness.

A recent lumped-mass model for a graphene-based microelectromechanical system is established in [21], taking into account the third order elastic-stiffness constant of the material. Furthermore, authors in [21] determine analytically the existence of periodic solutions, determine the static pull-in voltage, and then present a bifurcation analysis for this novel graphene-based MEMS model when a constant voltage is applied. For more related results about this model with constant voltage see [18,17,2].

Next, we introduce the central model of this paper, which is the damped non autonomous version of the one proposed in [21]. The device consists of two parallel plates separated by a distance d (known as gap), where one plate is fixed and the other is movable. The movable plate with mass m is attached to one end of a graphene strip, and in general the device is actuated by an input voltage. The mechanical axial displacement of the graphene strip (graphene-based material strip) is modeled as a nonlinear spring of length L. The figure 1 illustrates the idealized device.

Let E to denote the Young's modulus of graphene, D the absolute value of the third order elastic stiffness modulus of graphene, ϵ_0 the dielectric constant in free space, ϵ_r the relative permittivity of the gap space medium with respect to the free space, $\epsilon = \epsilon_0\epsilon_r$ the dielectric constant of the gap medium, A the movable plate area, A_c the graphene strip cross-sectional area, and x the axial displacement of the movable plate which is measured positive pointing down from its equilibrium position, i.e., from the position for which the distance between the plates is the gap d (see figure 1).

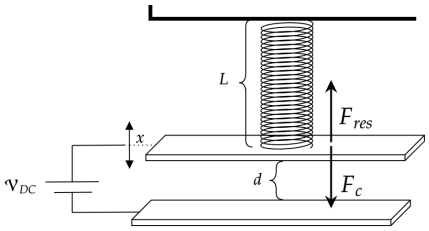

Fig. 1: Idealized parallel plates capacitor for the graphene-based MEM device with a constant input voltage $\mathcal{V}_{DC}$ (which can be replaced with a variable and periodic input voltage $\mathcal{V}(t)$).

Then the dimensional equation that rules the movement of the movable plate when we consider damping effects, and a damping coefficient c, is given by (see [21] and [8])

$$m\ddot{x} + c\dot{x} = F_{res} + F_c,$$

where

$$F_{res} = -EA_c\frac{x}{L} + DA_c\left|\frac{x}{L}\right|\frac{x}{L},$$

and

$$F_c = \frac{\epsilon A\mathcal{V}_{DC}^2}{2(d-x)^2},$$

are, respectively, the restoration and the electrostatic forces actuating over the device. When $\mathcal{V}_{DC}$ is replaced by a variable voltage $\mathcal{V}(t)$ the electrostatic force becomes

$$F_c = \frac{\epsilon A\mathcal{V}^2(t)}{2(d-x)^2}.$$

The restoration force F_{res} follows from the study of the graphene strip mechanical response proposed in [8], which takes into account the third-order elastic stiffness modulus for graphene, and the resulting isotropic elastic response of graphene given in [12]. The electrostatic force F_c is derived from the well known parallel plates electrostatic force (see [22]). Note that gravity effects have been neglected.

For modeling and numerical reasons it is advisable to define dimensionless variables by means of the following change of scales

$$\bar{x} = \frac{x}{d}, \quad \bar{t} = \omega_0 t,$$

where ω_0 is the natural frequency of the system and d is the gap. Returning to the original symbols we obtain as in [21] the following dimensionless equation

$$\ddot{x} + b\dot{x} + x - \alpha|x|x = \frac{\beta \mathcal{V}^2(t)}{(1-x)^2}, \tag{1}$$

where

$$b = c\sqrt{\frac{L}{EA_c m}} > 0, \;\; \alpha = \frac{Dd}{EL} > 0,$$

$$\beta = \frac{\epsilon AL}{2EA_c d^3} > 0 \;\text{ and }\; x < 1.$$

Here b denotes the dimensionless damping coefficient, and the parameters α and β relate the elastic properties of the material with the geometry of the device.

Then, the main purpose of this paper is to study analytically the existence and stability properties of periodic solutions of (1) when a periodic voltage with alternating current is applied. Thus, we obtain some sufficient conditions that lead to the existence of exactly three periodic oscillations with constant sign for the model presented above, being the central one asymptotically locally stable (Theorems 1 and 2). These results also show the rising of a fold bifurcation for periodic solutions like in [7]. Consequently, we provide a new insight into the dynamics of a graphene-based electrostatic micro actuator modeled by means of this non autonomous version of the novel graphene-based MEMS model from literature.

This paper is organized as follows. In section 2 we introduce some preliminary definitions and main results about existence, multiplicity and stability of periodic solutions for the graphene-based MEMS model. In section 3 we provide the proofs of our main results. Finally in section 4 we discuss some numerical results that highlight the advantages of using graphene, through comparison between a canonical linear elastic response MEMS model and the graphene-based MEMS model. For a better readability of this document we have included some auxiliary results in Appendixes A and B.

2 Main Results

In order to establish the main results of this paper we need first to consider some preliminaries. Notice that equation (1) can be rewritten as

$$\begin{gathered} \ddot{x} + f(t,x,\dot{x}) = 0, \\ f(t,x,\dot{x}) = b\dot{x} + x - \alpha|x|x - \frac{\beta \mathcal{V}^2(t)}{(1-x)^2}, \end{gathered} \tag{2}$$

with $f : \mathbb{R} \times]-\infty, 1[\times \mathbb{R} \to \mathbb{R}$ and $f \in C^1(\mathbb{R}/\mathrm{T}\mathbb{Z} \times]-\infty, 1[\times \mathbb{R})$. Additionally, here we consider a smooth positive and T-periodic input voltage function $\mathcal{V}(t)$. Thus we can define

$$\mathcal{V}_{min} := \min_{t\in[0,T]} \mathcal{V}(t) \;\text{ and }\; \mathcal{V}_{max} := \max_{t\in[0,T]} \mathcal{V}(t).$$

Along this paper we will consider two important auxiliary functions defined as follows.

For each $\alpha > 0$, let us define $\phi_\alpha : \mathbb{R} \to \mathbb{R}$ by

$$\phi_\alpha(x) = (x - \alpha|x|x)(1-x)^2.$$

This function will be referred to as the *auxiliary function* for equation (1). Notice that $\phi_\alpha \in C^1(\mathbb{R})$ and it has roots at $x = 0$, $x = \pm 1/\alpha$ and $x = 1$ (see figure 2). Additionally, the *auxiliary function* has exactly one negative local minimum in $]-\infty, 0[$ and a positive local maximum in $]0, S_\alpha[$ where

$$S_\alpha = \begin{cases} 1 & \text{if } 0 < \alpha \leq 1, \\ \dfrac{1}{\alpha} & \text{if } \alpha > 1. \end{cases}$$

We will tackle some properties and the importance of the *auxiliary function* ϕ_α.

Let us consider now $C_\alpha \in]0, S_\alpha[$ the unique critical point of ϕ_α, such that

$$\mathcal{K}_\alpha := \phi_\alpha(C_\alpha) = \max_{x\in]0,S_\alpha[} \phi_\alpha(x) > 0. \tag{3}$$

Indeed, a direct computation shows that

$$\mathcal{K}_\alpha = (512\alpha^3)^{-1}(-16\alpha^4 + 32\alpha^3 + 56\alpha^2 + (2\kappa^3 - 72)\alpha - \kappa^3 + 27),$$

with $\kappa = \sqrt{4\alpha^2 - 4\alpha + 9}$.

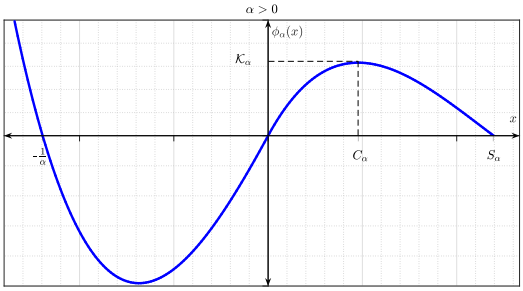

Fig. 2: *Auxiliary function* $\phi_\alpha(x)$.

On the other hand, for $M \in \left]0, (\frac{\pi}{T})^2\right[$ we define $G : \left[M, (\frac{\pi}{T})^2\right] \to \mathbb{R}$ as

$$G(\ell) = \frac{\ell - M}{\sqrt{\ell}} \cot\sqrt{\ell}\left(\frac{T}{2}\right), \tag{4}$$

for $M \le \ell \le \left(\frac{\pi}{T}\right)^2$.

Is is easy to verify that G is a continuous positive function vanishing only on the boundary. Therefore, we can define

$$b^*(M) := \max_{\ell\in\left[M,(\frac{\pi}{T})^2\right]} G(\ell).$$

Function G arises from the methodology and will be useful to apply Theorem 4 in Appendix A.

Notice that $\phi_\alpha(x) < 0$ in $\left]-\frac{1}{\alpha}, 0\right[\cup]S_\alpha, 1[$. Thus, if $0 < h_0 < \mathcal{K}_\alpha$ we obtain that the continuous function $h(x) = \phi_\alpha(x) - h_0$ has exactly one zero in $\left]-\infty, -\frac{1}{\alpha}\right[$, $]0, C_\alpha[$ and $]C_\alpha, S_\alpha[$, respectively, since h is strictly monotone and changes its sign over these intervals. If $h_0 = \mathcal{K}_\alpha$, then a similar argument implies that h has exactly one root in $\left]-\infty, -\frac{1}{\alpha}\right[$ and $]0, S_\alpha[$, respectively. Finally, if $h_0 > \mathcal{K}_\alpha$, then h has exactly one root in $\left]-\infty, -\frac{1}{\alpha}\right[$ (for a more intuitive graphical analysis reader can see figure 4).

Definition 1 Consider the *auxiliary function* ϕ_α and assume that $\beta\mathcal{V}_{max}^2 < \mathcal{K}_\alpha$. Thus, we denote the root in $]0, C_\alpha[$ of function h with $h_0 = \beta\mathcal{V}_{min}^2$ by x_{U1} and the root in $]0, C_\alpha[$ of function h with $h_0 = \beta\mathcal{V}_{max}^2$ by x_{L1}. Moreover, we define

$$b_\alpha^* = b^*(M),$$

with

$$M = \frac{\phi'_\alpha(x_{U1})}{(1 - x_{U1})^2}.$$

Now we are able to establish our main results.

Theorem 1 *Consider equation* (1) *and assume that*

1. *a)* $\beta\mathcal{V}_{max}^2 < \mathcal{K}_\alpha$, *b)* $0 < T \le \eta_\alpha$, *c)* $0 < b < \Gamma_\alpha$,

   where η_α *and* Γ_α *are given by*

   $$\eta_\alpha = \pi\frac{(1 - C_\alpha)}{\sqrt{\phi'_\alpha(x_{U1})}},$$

   and

   $$\Gamma_\alpha = \min\left\{2\frac{\sqrt{\phi'_\alpha(x_{L1})}}{(1 - x_{L1})}, b_\alpha^*\right\},$$

   with b_α^*, x_{U1} *and* x_{L1} *as in Definition 1. Then there exist at least three* T*-periodic solutions* $\psi(t)$, $\varphi_1(t)$ *and* $\varphi_2(t)$ *of* (1), *such that for all* $t \in [0, T]$

   $$\varphi_2(t) < 0 < \psi(t) < \varphi_1(t).$$

   Moreover, the solution $\psi(t)$ *is asymptotically locally stable, and the solution* $\varphi_2(t)$ *is unstable.*

2. $\beta \mathcal{V}_{max}^2 > \mathcal{K}_\alpha$,

Then there exists exactly a negative T-periodic solution $\hat{\varphi}(t)$ of (1) which is unstable.

Some additional restriction over the period T allows us to introduce a multiplicity result for positive T-periodic solutions and inquire about the stability properties of $\varphi_2(t)$.

Theorem 2 *Consider the equation (1), assume hypothesis 1 of Theorem 1 and that*

$$(1 - 2\beta \mathcal{V}_{min}^2) - \frac{b^2}{4} \leq \left(\frac{\pi}{T}\right)^2. \tag{5}$$

Then the problem (1) has exactly two positive T-periodic solutions $\psi(t)$, $\varphi_1(t)$ and exactly one negative T-periodic solution $\varphi_2(t)$, which are the solutions given by Theorem 1. Moreover, the solution $\psi(t)$ is asymptotically locally stable and $\varphi_1(t)$, $\varphi_2(t)$ are unstable.

Remark 1 For Theorem 2 we have that if

$$\mathcal{V}_{min}^2 \geq \frac{4 - b^2}{8\beta},$$

then condition (5) of Theorem 2 is easily satisfied. Furthermore, if

$$\mathcal{V}_{min}^2 < \frac{4 - b^2}{8\beta},$$

then the number

$$\eta := \frac{2\pi}{\sqrt{4 - b^2 - 8\beta \mathcal{V}_{min}^2}},$$

is real and positive. Thus, condition (5) is equivalent to the restriction over the period

$$0 < T \leq \eta,$$

i.e., the condition is basically like a high frequency result.

Figures 3a and 3b illustrate the existence results of this paper. Let us consider the parameters values of table 1 and a voltage function as in section 4.1, such that $\mathcal{V}_{DC} = 8\,\mathrm{V}$ and $\mathcal{V}_{AC} = 6\,\mathrm{V}$. Since the conditions of Theorem 2 hold we obtain the existence of exactly three T-periodic solutions $\psi(t)$, $\varphi_1(t)$ and $\varphi_2(t)$ for equation (1).

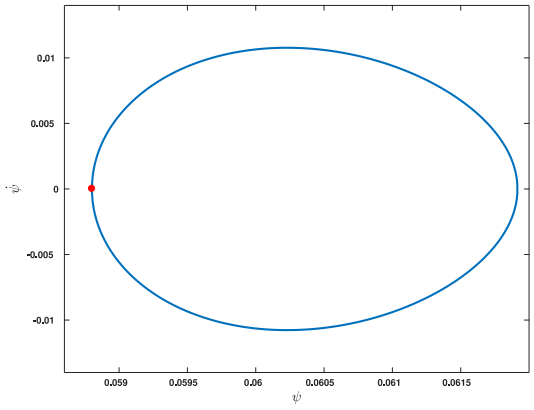

(a) Solution $\psi(t)$ in the $\psi\dot{\psi}$-plane with initial conditions $\psi(0) = 5.8801 \times 10^{-2}$ and $\dot{\psi}(0) = 1.9122 \times 10^{-5}$ (red dot).

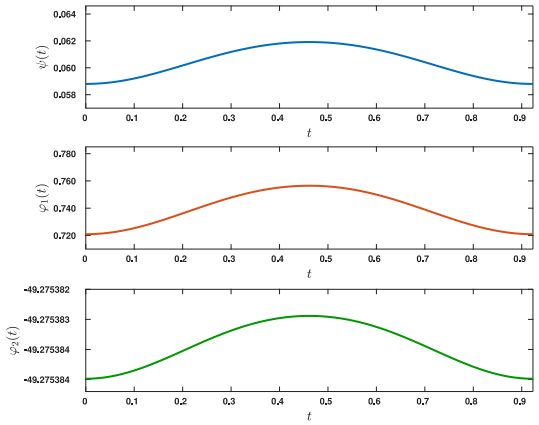

(b) T-periodic solutions $\psi(t)$, $\varphi_1(t)$ and $\varphi_2(t)$.

Fig. 3: Constant sign T-periodic solutions $\psi(t)$, $\varphi_1(t)$ and $\varphi_2(t)$ for equation (1) under conditions of Theorem 2.

We shall notice that simulations above were obtained by using the Matlab solver for boundary value problems *bvp5c* with a requested relative tolerance of 2.2204×10^{-14}, and a maximum error of 7.536×10^{-16} for solution $\psi(t)$, 8.089×10^{-12} for $\varphi_1(t)$ and 4.951×10^{-16} for $\varphi_2(t)$. Additionally, we notice that real solutions, i.e., solutions for the dimensional prob-

lem corresponding to solutions $\psi(t)$, $\varphi_1(t)$ and $\varphi_2(t)$, have a magnitude order of 1×10^{-8} m, 1×10^{-7} m and 1×10^{-5} m, respectively.

3 Proofs

The proofs of the main results are presented in this section. First we discuss some properties of the *auxiliary function* ϕ_α and its relevance along this section.

The auxiliary function. From definition of ϕ_α in section 1, it is easy to check that $\phi'_\alpha(0^+) = \phi'_\alpha(0^-) = 1$. Therefore, $\phi_\alpha \in C^1(\mathbb{R})$ with $\phi'_\alpha(0) = 1$. It is straightforward to verify that ϕ_α is decreasing on $]-\infty, -\frac{1}{\alpha}[$, increasing on $]0, C_\alpha[$ and then decreasing on $]C_\alpha, S_\alpha[$ again. Additionally, $\phi_\alpha(x) > 0$ on $]-\infty, -\frac{1}{\alpha}[\cup]0, S_\alpha[$, and $\phi_\alpha(x) < 0$ on $]-\frac{1}{\alpha}, 0[\cup]S_\alpha, 1[$.

An elementary computation shows that the positive critical point C_α defined in section 1 has the following analytic expression

$$C_\alpha = \frac{2\alpha + 3 - \sqrt{4\alpha^2 - 4\alpha + 9}}{8\alpha}.$$

On the other hand, for a T-periodic and variable input voltage the function ϕ_α is worthy for the existence study of T-periodic solutions. In fact, the x-coordinates of intersections of graph of the auxiliary function with horizontal lines, determinate the possible constant and non strict lower and upper solutions for the periodic problem (18) (see Appendix A). In other words, because Definition 2 in Appendix A, the non strict constant lower and upper solutions (denoted by x_L and x_U respectively) are the roots in $]-\infty, 1[$ of equations

$$\phi_\alpha(x_L) - \beta \mathcal{V}_{max}^2 = 0, \tag{6}$$

$$\phi_\alpha(x_U) - \beta \mathcal{V}_{min}^2 = 0. \tag{7}$$

The existence of such roots follows as particular cases from the existence of roots for the function h given in section 2. Figure 4 illustrates the *auxiliary function* and the location of non strict constant lower and upper solutions of (18) (see Appendix A) assuming that $\beta \mathcal{V}_{max}^2 < \mathcal{K}_\alpha$. Additionally, strict lower and upper solutions $\bar{L}$ and $\bar{U}$ can be viewed as solutions of the following inequalities

$$\phi_\alpha(\bar{L}) - \beta \mathcal{V}_{max}^2 > 0,$$

$$\phi_\alpha(\bar{U}) - \beta \mathcal{V}_{min}^2 < 0.$$

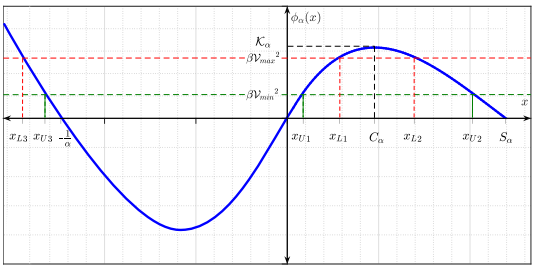

Fig. 4: *Auxiliary function* $\phi_\alpha(x)$, and location of lower and upper solutions assuming that $\beta \mathcal{V}_{max}^2 < \mathcal{K}_\alpha$.

Proof (Theorem 1) Notice that for equation (2) the function f can be written as

$$f(t, x, v) = bv + g(t, x),$$

with

$$g(t, x) = \frac{\phi_\alpha(x) - \beta \mathcal{V}^2(t)}{(1 - x)^2},$$

where $g : D \to \mathbb{R}$, $D = \mathbb{R} \times]-\infty, \mathrm{S}_\alpha[$, $g \in C^1(D)$ and g is T-periodic in t. We will consider throughout the proof the non strict constant lower and upper solutions of the periodic problem (18) (see Appendix A) for which (6), (7) hold respectively. We divide the proof in three steps (existence, uniqueness and stability) but before we make a necessary remark;

Remark 2 The hypothesis *1.b)* is equivalent to

$$\frac{\phi'_\alpha(x_{U1})}{(1 - C_\alpha)^2} \leq \left(\frac{\pi}{T}\right)^2.$$

Additionally, since $\phi'_\alpha(x_{L1}) > 0$ the number Γ_α is real, positive and satisfies

$$\Gamma_\alpha \leq 2\frac{\sqrt{\phi'_\alpha(x_{L1})}}{(1-x_{L1})} \quad \text{and} \quad \Gamma_\alpha \leq b^*_\alpha.$$

Then, hypothesis *1.c)* is equivalent to

$$0 < \frac{\phi'_\alpha(x_{L1})}{(1-x_{L1})^2} - \frac{b^2}{4} \quad \text{and} \quad 0 < b < b^*_\alpha.$$

Step 1. Existence of T-periodic solutions.

1. Assume hypothesis *1.a)* and consider the *auxiliary function* ϕ_α. Then there exist three roots for each equation (6) (L) and (7) (U) distributed as follows, $x_{L3} < x_{U3} < -1/\alpha < 0 < x_{U1} < x_{L1} < C_\alpha < x_{L2} < x_{U2} < S_\alpha$. Thus, we consider the following sets:

i) $\bar{E}_1 = \{(t,x,v) \in [0,T] \times]0, C_\alpha[\times \mathbb{R} \mid x_{U1} \leq x \leq x_{L1}\}$. Then f is continuous on $\bar{E}_1$ and $\partial_x f(t,x,v) = \partial_x g(t,x)$. Hence for $(t,x,v) \in \bar{E}_1$

$$\partial_x f(t,x,v) \leq (1 - 2\alpha x_{U1}) - \frac{2\beta\mathcal{V}^2_{min}}{(1-x_{U1})^3}.$$

Moreover, $\phi_\alpha(x_{U1}) = \beta\mathcal{V}^2_{min}$ and $\phi'_\alpha(x) = \left[4\alpha x^2 - (2\alpha+3)x + 1\right](1-x)$ for $x > 0$. This implies that

$$\begin{aligned}\partial_x f(t,x,v) &\leq \frac{4\alpha x_{U1}^2 - (2\alpha+3)x_{U1} + 1}{(1-x_{U1})} \\ &= \frac{\phi'_\alpha(x_{U1})}{(1-x_{U1})^2}.\end{aligned} \tag{8}$$

Since $\phi'_\alpha(x_{U1}) > 0$ we can set M as

$$M := \frac{\phi'_\alpha(x_{U1})}{(1-x_{U1})^2} < \frac{\phi'_\alpha(x_{U1})}{(1-C_\alpha)^2}. \tag{9}$$

Therefore, from hypothesis *1.b)* combined with Remark 2 we obtain that

$$\partial_x f(t,x,v) \leq M < \left(\frac{\pi}{T}\right)^2 \quad \text{on } \bar{E}_1.$$

On the other hand, $\partial_v f(t,x,v) = b$, and then assuming hypothesis *1.c)* we get from Remark 2 that $0 < b < b^*_\alpha$. Thus, a direct application of Theorem 4 in Appendix A with $N = b$ and $\ell = \ell^*$ a number in $]M, (\frac{\pi}{T})^2[$ such that $b^*_\alpha = G(\ell^*)$, implies the existence of at least one positive T-periodic solution ψ of problem (1) such that for all $t \in [0,T]$

$$x_{U1} \leq \psi(t) \leq x_{L1}.$$

ii) Let $\bar{E}_2 = \{(t,x,v) \in [0,T] \times]C_\alpha, S_\alpha[\times \mathbb{R} \mid x_{L2} \leq x \leq x_{U2}\}$. Notice that $f(t,x,v) = bv + g(t,x)$ satisfies the hypotheses of Theorem 3 in Appendix A on $\bar{E}_2$. Therefore, a direct application of Theorem 3 implies existence of at least one positive T-periodic solution $\varphi_1(t)$ of problem (1) such that for all $t \in [0,T]$

$$x_{L2} \leq \varphi_1(t) \leq x_{U2}.$$

iii) Let $\bar{E}_3 = \{(t,x,v) \in [0,T] \times]-\infty, -\frac{1}{\alpha}[\times \mathbb{R} \mid x_{L3} \leq x \leq x_{U3}\}$. Thus, a direct application of Theorem 3 as before implies existence of at least one negative T-periodic solution $\varphi_2(t)$ of problem (1) such that for all $t \in [0,T]$

$$x_{L3} \leq \varphi_2(t) \leq x_{U3}.$$

2. Assuming hypothesis *2)*, we can consider the following two cases: $\beta\mathcal{V}^2_{max} > \mathcal{K}_\alpha \geq \beta\mathcal{V}^2_{min}$ and $\beta\mathcal{V}^2_{min} > \mathcal{K}_\alpha$. It is easy to verify that for both cases there exists exactly one root for each equation (6) and (7), such that $x_L < x_U < -\frac{1}{\alpha}$. Let $\bar{E} = \{(t,x,v) \in [0,T] \times]-\infty, -\frac{1}{\alpha}[\times \mathbb{R} \mid x_L \leq x \leq x_U\}$, thus Theorem 3 implies existence of at least one T-periodic solution $\hat{\varphi}(t)$ of problem (1) such that for all $t \in [0,T]$

$$x_L \leq \hat{\varphi}(t) \leq x_U.$$

Step 2. Uniqueness of negative T-periodic solutions.

Now we shall prove that if *1)* holds then $\varphi_2(t)$ is the unique negative T-periodic solution of problem (1).

Assume that $x(t)$ denotes a T-periodic solution of (1) such that $x(t) < 0$ for all $t \in [0,T]$. Since $x(t)$ is a continuous function there exist

t_0, $t_1 \in [0,T]$ so that $\underline{x} = x(t_0) = \min_{t\in[0,T]} x(t)$ and $\overline{x} = x(t_1) = \max_{t\in[0,T]} x(t)$. Then $\dot{x}(t_0) = \dot{x}(t_1) = 0$ and this implies

$$0 \leq \ddot{x}(t_0) = -g(t_0,\underline{x}) = \frac{\beta\mathcal{V}^2(t_0) - \phi_\alpha(\underline{x})}{(1-\underline{x})^2}.$$

From here $\phi_\alpha(\underline{x}) \leq \beta\mathcal{V}_{max}^2$ and therefore $x_{L3} \leq \underline{x}$ (see figure 4). Similarly, we have that $0 \geq \ddot{x}(t_1) = -g(t_1,\overline{x})$, thus $\phi_\alpha(\overline{x}) \geq \beta\mathcal{V}_{min}^2$ and therefore $x_{U3} \geq \overline{x}$ (see figure 4). Hence we obtain that any negative T-periodic solution of problem (1) satisfies

$$x_{L3} \leq x(t) \leq x_{U3}.$$

Suppose now that there exists other negative T-periodic solution $\varphi_3(t)$ of problem (1). Thus, $x_{L3} \leq \varphi_3(t) \leq x_{U3}$ for all $t \in [0,T]$. Let us define $u(t) = \varphi_2(t) - \varphi_3(t)$ and notice that $u(t)$ satisfies

$$\ddot{u}(t) + b\dot{u}(t) + \hat{a}(t)u(t) = 0, \tag{10}$$

where $\hat{a}(t) = \dfrac{g(t,\varphi_2(t)) - g(t,\varphi_3(t))}{\varphi_2(t) - \varphi_3(t)}$ if $\varphi_2(t) \neq \varphi_3(t)$ and $\hat{a}(t) = \partial_x g(t,\varphi_2(t))$ if $\varphi_2(t) = \varphi_3(t)$.

Since g is of class C^1 on D, and $g(t,\cdot)$, $\varphi_2(t)$, $\varphi_3(t)$ are T-periodic functions, it is easy to verify that $\hat{a}(t) \in C(\mathbb{R}/\mathrm{T}\mathbb{Z})$. Furthermore, for $x < 0$

$$\partial_x g(t,x) = (1+2\alpha x) - \frac{2\beta\mathcal{V}^2(t)}{(1-x)^3}.$$

Since $1+2\alpha x < 0$ whenever $x < -\frac{1}{2\alpha}$, we have that $\partial_x g(\cdot,x) < 0$ on $[x_{L3}, x_{U3}]$ because $x_{U3} < -\frac{1}{\alpha}$. So, the Mean Value Theorem implies that for all $t \in \mathbb{R}$

$$\hat{a}(t) < 0.$$

Finally, equation in (10) can not admit non-trivial T-periodic solutions as consequence of Lemma 3 in Appendix B, therefore $\varphi_2(t)$ is the unique negative T-periodic solution of problem (1).

The uniqueness for negative T-periodic solutions assuming hypothesis *2)* is straightforward following the precedent ideas.

Step 3. Stability properties.

1. Assume hypothesis *1)* and consider $\bar{E}_1$. Thus, variational equation along solution $\psi(t)$ is given by

$$\ddot{y_1} + b\dot{y_1} + a_1(t)y_1 = 0, \tag{11}$$

where $a_1(t) = \partial_x g(t,\psi(t))$. Additionally, $a_1(t)$ is a T-periodic, continuous and not identically zero function. Therefore, using the first part of Lemma 2 in Appendix B we obtain the equivalent Hill's equation

$$\ddot{z}_1 + Q(t)z_1 = 0, \tag{12}$$

where $z_1(t) = \mathrm{e}^{\frac{1}{2}bt}y_1(t)$ and $Q(t) = a_1(t) - \frac{b^2}{4}$.

Notice that $Q(t)$ is T-periodic, continuous and satisfies for all $t \in [0,T]$ that

$$1 - 2\alpha x_{L1} - \frac{2\beta\mathcal{V}_{max}^2}{(1-x_{L1})^3} - \frac{b^2}{4} \leq a_1(t) - \frac{b^2}{4} < a_1(t).$$

Since x_{L1} y x_{U1} satisfy, respectively, $\phi_\alpha(x_{L1}) = \beta\mathcal{V}_{max}^2$ and $\phi_\alpha(x_{U1}) = \beta\mathcal{V}_{min}^2$, it follows that

$$1 - 2\alpha x_{L1} - \frac{2\beta\mathcal{V}_{max}^2}{(1-x_{L1})^3} = \frac{\phi'_\alpha(x_{L1})}{(1-x_{L1})^2},$$

Thus, the function $Q(t)$ satisfies

$$\frac{\phi'_\alpha(x_{L1})}{(1-x_{L1})^2} - \frac{b^2}{4} \leq Q(t) < a_1(t),$$

and assuming hypothesis *1.b)* and *1.c)*, we obtain as consequence of Remark 2 and (8) that

$$0 < Q(t) < M := \frac{\phi'_\alpha(x_{U1})}{(1-x_{U1})^2} < \left(\frac{\pi}{T}\right)^2,$$

for M defined in (9). Then an application of Proposition 2 in Appendix B shows that equation (12) is elliptic. Moreover, second part of Lemma 2 in Appendix B implies that characteristic multipliers of (11) are inside of the unit disk. The conclusion follows from linearization

principle.

2. Assume hypothesis *1.a)* of Theorem 1, thus we know that on $\bar{E}_3$ there exists exactly one negative T-periodic solution $\varphi_2(t)$ of problem (1), which has its range included in $[x_{L3}, x_{U3}]$. On the other hand, from the continuity and the decreasing character of ϕ_α on $\left]-\infty, -\frac{1}{\alpha}\right[$ one has the existence of $\epsilon > 0$ such that $\phi_\alpha(x_{L3} - \epsilon) - \beta\mathcal{V}^2_{max} > 0$ and $\phi_\alpha(x_{U3} + \epsilon) - \beta\mathcal{V}^2_{min} < 0$. Hence $\bar{L} = x_{L3} - \epsilon$ and $\bar{U} = x_{U3} + \epsilon$ are, respectively, strict constant lower and upper solutions of (18) (see Appendix A). The conclusion follows applying Proposition 1 in Appendix A.

A similar procedure, assuming hypothesis *2)* implies that the T-periodic solution $\hat{\varphi}(t)$ of the problem (1) is unstable. This completes the proof.

Remark 3 In practice, if the inequality in condition *1.b)* is strict, then we can choose ℓ in Theorem 4 as

$$\ell = \frac{\phi'_\alpha(x_{U1})}{(1 - C_\alpha)^2},$$

in order to obtain an easily computable Γ_α since (9) holds. Furthermore, b^*_α can be replaced by $G(\ell)$.

Remark 4 The proof of Theorem 1 also provides us *a posteriori* bounds over the found T-periodic solutions $\psi(t)$, $\varphi_1(t)$ and $\varphi_2(t)$. Thus assuming hypothesis *1)* we obtain that

$$\begin{aligned} &x_{L3} \le \varphi_2(t) \le x_{U3} < 0 < x_{U1} \\ &\le \psi(t) \le x_{L1} < x_{L2} \le \varphi_1(t) \le x_{U2}, \end{aligned}$$

where x_{L1}, x_{U1}, x_{L2}, x_{U2}, x_{L3} and x_{U3} are defined as in proof of Theorem 1.

Proof (Theorem 2) Assume hypothesis *1)* of Theorem 1. Then a direct application of Theorem 1 implies the existence of at least three T-periodic solutions $\psi(t)$, $\varphi_1(t)$ and $\varphi_2(t)$ of problem (1), that are located as in Remark 4. Moreover, we know that solution $\psi(t)$ is locally asymptotically stable and that solution $\varphi_2(t)$ is unstable and the unique negative T-periodic solution. Thus, it remains to prove that $\psi(t)$ and $\varphi_1(t)$ are the only two positive T-periodic solutions and that solution $\varphi_1(t)$ is unstable. We divide the proof in two steps.

Step 1. Multiplicity.

Let $D = \mathbb{R} \times]0, 1[$, then g is continuous on D and for all $(t, x) \in D$ we have that

$$\partial_x g(t, x) = (1 - 2\alpha x) - \frac{2\beta\mathcal{V}^2(t)}{(1 - x)^3} < 1 - 2\beta\mathcal{V}^2_{min}.$$

Therefore, assuming hypothesis (5) of Theorem 2 we obtain that

$$\partial_x g(t, x) < \left(\frac{\pi}{T}\right)^2 + \frac{b^2}{4} \quad \text{on } D.$$

Additionally, for all $(t, x) \in D$ it verifies

$$\partial^2_x g(t, x) = -2\alpha - \frac{2\beta\mathcal{V}^2(t)}{(1 - x)^4} < 0.$$

Finally, since $E_1 \cup E_2 \subset D$ for $E_1 = \{(t, x) \in [0, T] \times]0, C_\alpha[\mid x_{U1} \le x \le x_{L1}\}$ and $E_2 = \{(t, x) \in [0, T] \times]C_\alpha, S_\alpha[\mid x_{L2} \le x \le x_{U2}\}$, the application of second part of Lemma 1 in Appendix A implies that $\psi(t)$ and $\varphi_1(t)$ are the only T-periodic solutions of (1) in $]0, 1[$.

Step 2. Instability of $\varphi_1(t)$.

Assume the hypothesis of Theorem 2, then we know that there exists exactly one positive T-periodic solution $\varphi_1(t)$ of (1), which has its range included in $[x_{L2}, x_{U2}]$. On the other hand, we have that a similar argument on $]C_\alpha, S_\alpha[$ as in step 3 of the proof of Theorem 1 leads to the existence of a small $\epsilon > 0$ such that $\bar{L} = x_{L2} - \epsilon > C_\alpha$ and $\bar{U} = x_{U2} + \epsilon$ are, respectively, strict constant lower and upper solutions of (1) (see definition above). Thus, conclusion follows from Proposition 1 in Appendix A since we know that $\varphi_1(t)$ is the unique T-periodic solution such that for all $t \in [0, T]$

$$\bar{L} < \varphi_1(t) < \bar{U}.$$

This completes the proof.

4 Numerical Results: application to a graphene-based micro actuator

In this section we present some numerical results for a graphene-based micro actuator modeled by the damped non autonomous version of the graphene-based MEMS model introduced in section 1. Thus, we aim to verify theoretical results obtained in previous sections and to show some gains of using graphene by means of a comparison between the nonlinear elastic response model of this paper and the linear elastic response parallel plates MEMS model (Nathanson's model). First we justify the parameter values used in the simulations and then we compare the two models.

4.1 Parameters values for the graphene MEMS model

In this section we summarize the parameter values for the numerical results starting with the mechanical response of the graphene. The experimental values of the second order and third order elastic stiffness modulus for 2D monolayer graphene can be found in [12]. Thus, assuming a graphene thickness of 0.335 nm (see [12]) we obtain the corresponding values of $E = 1.0(1)$ TPa and $D = 2.0(4)$ TPa. These are the values that we will use in our computations.

Table 1 contains realistic values of the parameters that are employed to obtain the numerical results for the graphene-based MEMS model, when a voltage $\mathcal{V}(t) = \mathcal{V}_{DC} + \mathcal{V}_{AC}\cos(\hat{\omega}t)$ is supplied (see equation (1)). Notwithstanding, we notice that $\mathcal{V}_{DC}$ and $\mathcal{V}_{AC}$ can be tuned to convenience almost like "control parameters" to explore the dynamical behavior of the system as long as the required conditions from main theorems hold. In section 4.2 we will consider $\mathcal{V}_{DC} = 5\,\mathrm{V}$ and $\mathcal{V}_{AC} = 3\,\mathrm{V}$, and later in section 4.4 we will consider $\mathcal{V}_{DC} = 3\,\mathrm{V}$ and $\mathcal{V}_{AC} = 1.5\,\mathrm{V}$.

Table 1: Parameters values.

β	$6.510\,432\,214\,911\,766 \times 10^{-4}\,\mathrm{V}^{-2}$
α	$2.029\,411\,764\,705\,882 \times 10^{-2}$
b	$1.153\,802\,627\,922\,852 \times 10^{-2}$
$\hat{\omega}$	$6.806\,139\,097\,297\,727$
T	$9.231\,643\,986\,932\,663 \times 10^{-1}$

4.2 Numerical continuation results

The theoretical results of previous section establish the existence of a stable and an unstable solution coexisting for the same value of the parameters provided some conditions are fulfilled (see Theorem 1). In this section we present numerical continuation results as one of the parameters is changed using AUTO which is a well tested and powerful program to analyze (among others) periodic solutions of dynamical systems [10].

Figure 5 shows the bifurcation diagram where the primary continuation parameter is the amplitude of the forcing $\mathcal{V}_{AC}$ for a fixed value of the DC voltage $\mathcal{V}_{DC} = 5V$. The blue hollow square at $\mathcal{V}_{AC} = 3$ is the starting solution of the diagram which is stable and was computed numerically solving a boundary value problem with the parameters and boundary value inferred from Theorem 1. As the branch (solid line) moves to higher values of $\mathcal{V}_{AC}$ the stability is preserved up to a critical value at which a limit point occurs (LP) (red asterisk). At this point the branch becomes unstable (dashed line) and the value of the continuation parameter diminishes until a vanishing value of the alternating voltage is reached. The vertical axis is the norm of the solution averaged over a period [10] and is just a a scalar measure for the bifurcation diagram. Note that the equilibria for $\mathcal{V}_{AC} = 0$ (one stable and another unstable) can be analytically computed for the autonomous case. The symmetric shape of the negative $\mathcal{V}_{AC}$ part of the bifurcation diagram is to be expected since the sign of alternating forcing does not play a role in the bifurcation

behavior.

Two solutions close to the LP ($V_{AC} = 19.9$ (black squares)) has been selected and correspond to the stable and unstable solutions predicted by the theorem. They will also appear in the stroboscopic Poincaré plot of the next section. The linear stability around these periodic solution is measured by the corresponding Floquet multipliers and can be relevant for the applications.

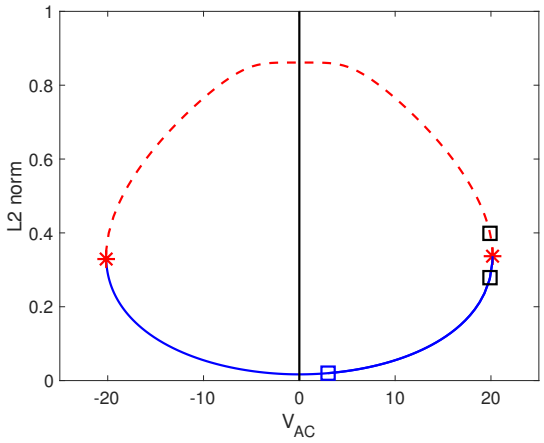

Fig. 5: Bifurcation diagram computed with AUTO using a pseudo arc length continuation scheme. The blue solid line is the stable part of the branch whereas the red dashed curve is the unstable one. The blue hollow square is the starting solution at $\mathcal{V}_{AC} = 3$, the two black squares at $\mathcal{V}_{AC} = 19.9$ are a stable (lower) and unstable (upper) solutions close to the limit point (red asterisks) where the branch changes its stability.

Figure 5 is a numerical implementation of Theorem 1: when the parameter lies in the appropriate interval we find two periodic solutions with opposite stability that live always in the positive part of x. Outside of the region no periodic solutions can be predicted and the separating case occurs exactly where the stable and the unstable periodic solution merge at a fold bifurcation.

In figure 6 we present the phase space representation of the positive solution exactly at the Limit Point in the bifurcation diagram.

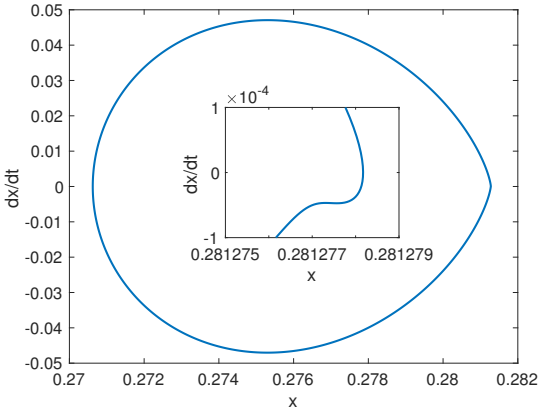

(a) Phase space representation of the positive solution at the Limit Point in the bifurcation diagram. The vertical axis is the velocity whereas the horizontal axis is the position. The inset is a zoom close to the rightmost part of the orbit.

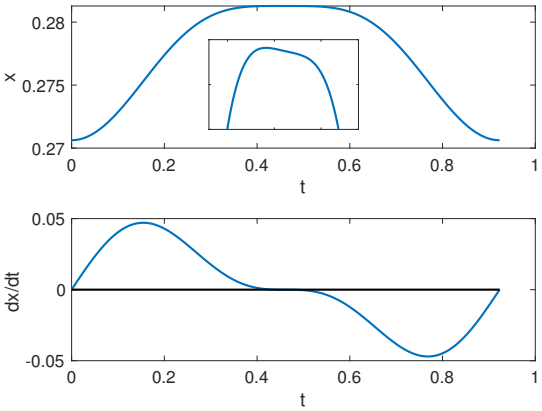

(b) Position (upper) with a zoom around the maximum value and velocity (lower) of the solution that is undergoing a Limit Point bifurcation.

Fig. 6: Phase space representation of the positive solution at the Limit Point in the bifurcation diagram, for this value of the $\mathcal{V}_{AC}$ parameter (20.1673) the stable and unstable solution merge and the conditions of Theorem 1 are not fulfilled.

We notice that the zoom close to the rightmost end of the curves shows a highly non symmetric and nonlinear behavior of the oscillation of the plate of the graphene MEMS. The solutions are always far enough from the singularity at $x = 1$.

4.3 Stroboscopic map

In this section we present some results to illustrate the stability and basins of attraction of the periodic solution by means of a stroboscopic Poincaré map both for the graphene and traditional MEMS only for the positive T-periodic solutions. The stroboscopic maps have been computed by accurately integrating forward and backwards in time with initial conditions close to the orbits of interest but keeping the position and velocity values only for integer time multiples of the period of the external forcing. We have used Matlab solver *ode45* with tolerances of the order of 10^{-14}.

The dynamical behavior of the trajectories can be visualized using of two different color-maps with four colors each and two different time direction integrations. Color-bar A goes from green to blue and the trajectories remain one quarter of the time at each successive color in a forward time integration. The initial conditions for this case have been selected in a grid around to the stable equilibrium point. Color-bar B runs from yellow to red with the same convention (a quarter of the total time at each sub color) in a backwards time integration close to the unstable equilibrium point.

Figure 7a shows the region of interest of the stroboscopic map when $\mathcal{V}_{AC} = 19.9\,\mathrm{V}$, with a mesh grid of 10200 nodes for the fixed point on the left, and a mesh grid of 1270 nodes for the fixed point on the right. Trajectories corresponding to the mesh grid of the fixed point on the left are portrayed with color-bar A, and those corresponding to the mesh grid of the fixed point on the right with the color-bar B. The integration in the first case was to $3000T$ and in the second case was to $-3000T$. Figure 7b is a close up to the map that shows the existence of a region containing the fixed point on the left, for which the trajectories have an asymptotic behavior to that fixed point. This region also seems to be bounded by some of the trajectories corresponding to the mesh of the fixed point on the right. We notice the existence of trajectories that escape towards the singularity, resulting in a possible blow-up behavior.

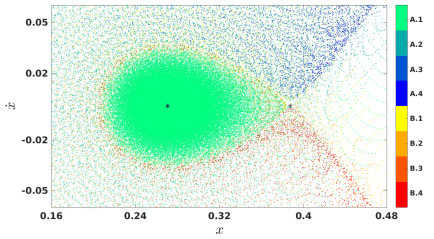

(a) Region of interest of the stroboscopic map with a typical fish-like figure.

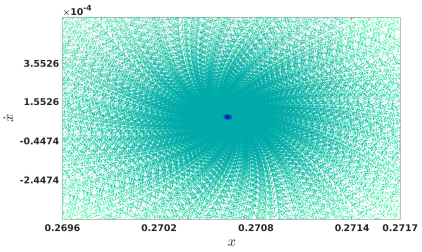

(b) Close up to the central region of the stroboscopic map.

Fig. 7: Region of interest of the stroboscopic map and close up associated to the case $\mathcal{V}_{AC} = 19.9\,\mathrm{V}$. In 7a the desired experimental region is the green stable lobe around the stable periodic solution. A separatrix curve can also be observed separating the stable and unstable regimes. The unstable equilibrium point has two unstable and two stable directions.

A typical fish-like figure is formed around the stable-unstable equilibrium couple. As expected the green "fish" shrinks at the fold bifurcation and disappears. Note that from the applications point of view the region of interest is

precisely the stable basin of attraction and the unstable initial conditions have to be avoided.

Figure 8 shows the region of interest of the stroboscopic map when $\mathcal{V}_{AC} = 4.5\,\mathrm{V}$ by using the same colour-maps as in the former case, a mesh grid of 10200 nodes with a perturbation parameter of 1.95×10^{-2} for the fixed point on the left, and a mesh grid of 7675 nodes with a perturbation parameter of 3.46×10^{-3} for the fixed point on the right. The conditions of Theorems 1 and 2 are satisfied, thus as the previous section shows, one of the positive T-periodic solutions is asymptotically locally stable and the other is unstable. Thus, we obtain the existence of a region of initial conditions for which trajectories have an asymptotic behavior to the fixed point on the left, moreover, this region is completely bounded by some of the trajectories with initial conditions nearby the fixed point of the right. Note that for this case the basin of attraction has increased significantly. This fact could be anticipated from the numerical continuation diagram 5 by looking at the distance between the two equilibria. In some sense the continuation and the stroboscopic diagrams provide complementary information about the dynamical behavior of the solutions.

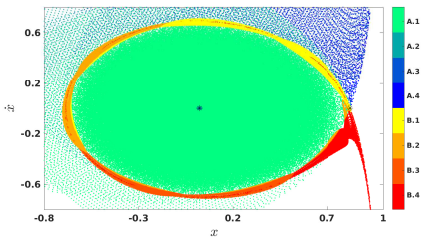

Fig. 8: Region of interest of the stroboscopic map associated to the case $\mathcal{V}_{AC} = 4.5\,\mathrm{V}$.

4.4 Basin of Attraction Comparison

In this section, we compare the basins of attraction (see [22]), of the two MEMS models, paying special attention to the robustness properties.

In order to tackle the comparison between the two models we need to ensure equivalent operating conditions. Therefore we will use in both models the same gap, area of the plates, damping coefficient, and the geometry of a parallel plates device. Additionally, we will take into account for the Nathanson's model a linear restoration force as follows.

$$\overline{F}_{res} = -\overline{E} A_c \frac{x}{L},$$

where A_c, L and x are defined as in section 1, and $\overline{E}$ denotes the Young's modulus of some material, for example, the silicon. Hence we consider $\overline{E} = 100\,\mathrm{GPa}$. On the other hand, to achieve the comparison we ensure the existence of two periodic solutions for the linear response model through the application of lower and upper solutions theorems, moreover, one of them is asymptotically locally stable. Before we present the results of this section we notice that the stroboscopic map associated to the linear response model has been shifted so that fixed points corresponding to the asymptotically locally periodic solutions for both models match.

We notice that for a periodic input voltage with $\mathcal{V}_{DC} = 3\,\mathrm{V}$ and $\mathcal{V}_{AC} = 1.5\,\mathrm{V}$, figures 9a and 9c show the region of interest of the stroboscopic map associated to both models. For the case of the nonlinear response model, we consider a mesh grid of 3720 nodes, and perturbation parameters of 3.305×10^{-2} for the fixed point on the left and 3.065×10^{-3} for the fixed point on the right. On the other hand, for the case of the linear response model we consider a mesh grid of 3720 nodes with a perturbation parameter of 3.06×10^{-2} for the fixed point on the left, and a mesh grid of 1580 nodes with a perturbation parameter of 1.035×10^{-2} for the fixed point on the right. Additionally, trajectories corresponding to the mesh grid of the fixed point on the left are portrayed with colormap C, and those corresponding to the mesh

grid of the fixed point on the right with the color-map D. Figure 9b is a close up to figure 9a, and figure 9d is a close up to figure 9c.

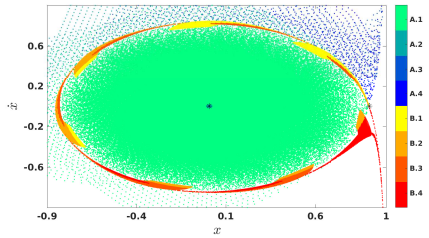

(a) Region of interest for the nonlinear response model.

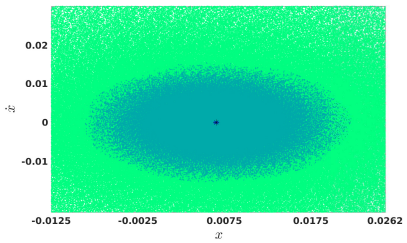

(b) Close up to the region of interest for the nonlinear response model.

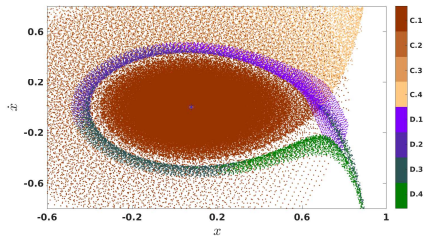

(c) Region of interest for the linear response model.

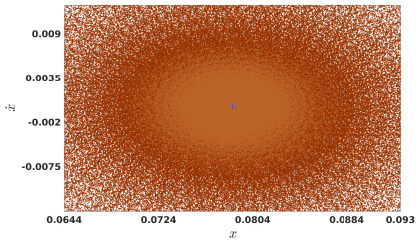

(d) Close up to the region of interest for the linear response model.

Fig. 9: Region of interest of the stroboscopic map associated to both models.

The size of the basin of attraction for the graphene-based MEMS is considerably larger than for the classical silicon based MEMS (please note the different scales).

Figure 10 gives an insight into the comparison between the two models considering dimensional variables. We can observe that the set of initial conditions that leads to a good operation of the device, i.e., the safe operation region, of the model with nonlinear response is greater than the safe operation region of the model with linear response.

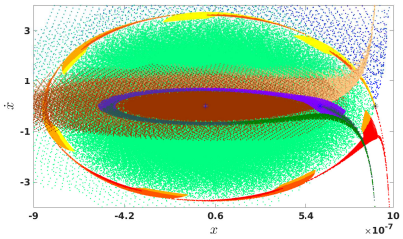

Fig. 10: Comparison between the regions of interest of the stroboscopic maps associated to the models with nonlinear and linear elastic response for $\mathcal{V}_{DC} = 3\,\mathrm{V}$ and $\mathcal{V}_{AC} = 1.5\,\mathrm{V}$.

5 Concluding remarks

We provide sufficient conditions that give an insight into the existence and the stability properties of constant sign periodic oscillations for the graphene-based MEMS when a non constant periodic voltage is supplied. Specifically, under some conditions we obtain the existence of exactly three constant sign periodic oscillations, one of them is negative and the others are positive in sign. Furthermore, the positive one in the middle is asymptotically locally stable and the others are unstable. These results could be an approach to a design principle for stabilizing the microelectronic device without an external controller, since a proper adjustment of the input voltage leads to a required operation whenever the damping coefficient is

under a certain quantity.

We notice that numerical continuation results provide a region of values for which the amplitude of the alternating forcing can range, ensuring that we can still obtain a stable operating regime of the device. Moreover, these results give numerical evidence of a fold bifurcation of positive periodic solutions when a periodic input voltage is considered. On the other hand, numerical simulations show one of the advantages granted by the graphene when it is considered as a material for MEMS. Specifically, from a lumped-mass model approach, we do observe that under proper conditions on the control parameters and ensuring same operating conditions, the safe operation region of the graphene-based MEMS is greater than the safe operation region of a canonical MEMS for a parallel plates capacitor.

We point out that our results comprehend constant sign periodic solutions and thus we do not know if there exist variable sign periodic solutions that correspond to oscillations where the movable plate passes through its relaxed position, i.e., when distance between both fixed and movable plate is the gap d. Therefore, a future work is to provide a global multiplicity result that reveals if there exist more periodic solutions besides those of constant sign studied here by following the ideas in [7]. Then we expect to provide an analytical proof for the existence of a fold bifurcation of periodic solutions for the graphene-based MEMS model when a parameter, e.g., the gap d, is changed.

Application to the dimensional graphene-based MEMS model: Now we discuss our results for the graphene-based electrostatic parallel plates micro actuator which has associated the following dimensional equation

$$m\ddot{x} + c\dot{x} + EA_c\frac{x}{L} - DA_c\left|\frac{x}{L}\right|\frac{x}{L} = \frac{\epsilon A V(t)^2}{2(d-x)^2},$$

where $V(t)$ is a $\mathcal{T}$-periodic input voltage such that

$$V_{max} := \max_{t\in[0,\mathcal{T}]} V(t) \quad \text{and} \quad V_{min} := \min_{t\in[0,\mathcal{T}]} V(t).$$

and the parameters E, D, ϵ, A, A_c, and the variable x are defined as in section 1.

Thus the hypothesis *1.a)* is equivalent to the following restriction

$$V_{max} < \sqrt{\frac{2\mathcal{K}_\alpha EA_c d^3}{\epsilon AL}}. \tag{13}$$

The hypothesis *1.b)* is equivalent to the following restriction over the period $\mathcal{T}$

$$0 < \mathcal{T} \leq \frac{\eta_\alpha}{\omega_0}, \tag{14}$$

where

$$\omega_0 = \sqrt{\frac{EA_c}{Lm}},$$

denotes the natural frequency of the system, as the nondimensionalization process reveals. Then, the input voltage frequency denoted by ω should satisfy

$$\omega \geq \frac{\omega_0}{\eta_\alpha}.$$

Finally, hypothesis *1.c)* implies a restriction over the damping coefficient, such that

$$0 < c < \Gamma_\alpha\sqrt{\frac{EA_c m}{L}}. \tag{15}$$

To sum up, we obtain under conditions (13), (14) and (15) that high enough AC voltage frequencies lead to stabilization of the micro-electromechanical system with a periodic oscillation of the movable plate. Indeed there will be at least three lateral $\mathcal{T}$-periodic oscillations, and at least two of them will be positive. Imposing the following additional condition we obtain the existence of exactly two positive oscillations

$$\left(1 - \frac{\epsilon AL}{EA_c d^3}V_{min}^2\right) - \frac{c^2 L}{4EA_c m} \leq \left(\frac{\pi}{\omega_0\mathcal{T}}\right)^2, \tag{16}$$

which will be equivalent to the restriction

$$\mathcal{T} \leq \frac{2\pi}{\omega_0}\sqrt{\frac{EA_c md^3}{4EA_c md^3 - L(c^2d^3 + 4\epsilon A m V_{min}^2)}},$$

whenever

$$V_{min}^2 < \frac{EA_c d^3}{\epsilon AL} - \frac{c^2 d^3}{4\epsilon Am}.$$

Finally, we notice that the condition (16) implies also that the positive oscillation nearest to the fixed plate won't be observable since it will be unstable. Moreover, we know the existence of a negative and unstable oscillation, nevertheless, we do not know if it is "always" physically possible since in this case the material seems to have other regime of elastic response.

Acknowledgements The author D. Núñez was financially supported by the Capital Semilla (2019-2020) project 020100654 and the author J. Galán-Vioque was financially supported by Spanish Grants PGC2018-096265-BI00 and PGC2018-100680-B-C21.

Conflict of interest

The authors declare that they have no conflict of interest.

Availability of data and material

'Not applicable'.

Code availability

'Not applicable'.

Appendix A: Lower and Upper Solutions Theory

Now we introduce some classical results about Lower and Upper solutions Method. Consider the second order differential equation of the form

$$\ddot{x} + f(t, x, \dot{x}) = 0, \tag{17}$$

where $f : \bar{D} \to \mathbb{R}$ and $f \in C^1(\bar{D})$ with $\bar{D} = \mathbb{R} \times]\mathrm{x}_1, \mathrm{x}_2[\times \mathbb{R} \subset \mathbb{R}^3$ and $-\infty < \mathrm{x}_1 < \mathrm{x}_2 < \infty$. Assume that f is T-periodic in variable t. It is well known fact that the problem of finding periodic solutions of (17) is equivalent to solve the periodic boundary problem

$$\begin{aligned} &\ddot{x} + f(t, x, \dot{x}) = 0, \\ &x(0) = x(T),\ \dot{x}(0) = \dot{x}(T). \end{aligned} \tag{18}$$

Definition 2 ([4]) A function $L \in C^2(]0, T[) \cap C^1([0, T])$ is a lower solution of the periodic problem (18) if for all $t \in [0, T]$

1. $\ddot{L}(t) + f(t, L(t), \dot{L}(t)) \geq 0$,
2. $L(0) = L(T),\ \dot{L}(0) \geq \dot{L}(T)$.

A function $U \in C^2(]0, T[) \cap C^1([0, T])$ is an upper solution of periodic problem (18) if for all $t \in [0, T]$ the inequalities in 1 and 2 hold with reversed order. When the inequalities in 1 and 2 are strict the corresponding lower (upper resp.) solution is called strict.

We assume that the lower and upper solutions of the periodic problem (18) have range in $]\mathrm{x}_1, \mathrm{x}_2[$. Next we present some needed versions of existence results. The following result is a direct consequence of Theorem 5.2 in chapter 1 of [4].

Theorem 3 *Let L and U be lower and upper solutions of the periodic problem* (18) *such that $L(t) \leq U(t)$ for all $t \in [0, T]$. Define $\bar{E}$*

$$\bar{E} = \{(t, x, v) \in [0, T] \times \mathbb{R}^2 \mid L(t) \leq x \leq U(t)\},$$

and assume that $f : \bar{E} \to \mathbb{R}$ is a continuous function of the form

$$f(t, x, v) = bv + p(t, x),$$

where $p(t, x)$ is a real value function bounded on $\hat{E} = \{(t, x) \in [0, T] \times \mathbb{R} \mid L(t) \leq x \leq U(t)\}$ and $b > 0$. Then there exists at least one solution $x(t) \in C^2([0, T])$ of the periodic problem (18) *such that for all $t \in [0, T]$*

$$L(t) \leq x(t) \leq U(t).$$

A particular case of Theorem 3.2 in chapter 5 of [4], about lower and upper solutions in reversed order, is easily obtained for constant lower and upper solutions and f regular enough.

Theorem 4 *Let L and U be constant lower and upper solutions of the periodic problem* (18) *such that $U < L$, define*

$$\bar{E} = \{(t, x, v) \in [0, T] \times \mathbb{R}^2 \mid U \leq x \leq L\},$$

and assume that $f : \bar{E} \to \mathbb{R}$ is continuous with continuous partials derivatives on $\bar{E}$. Suppose that there exists $M \in \left]0, (\frac{\pi}{T})^2\right[$ such that

$$\partial_x f(t, x, v) \leq M \quad \text{for all} \quad (t, x, v) \in \bar{E},$$

that there exists $N > 0$ *so that*

$$|\partial_v f(t, x, v)| \leq N \quad \text{for all} \quad (t, x, v) \in \bar{E},$$

and let $\ell \in \left]M, (\frac{\pi}{T})^2\right[$ such that

$$N \leq G(\ell),$$

with G the auxiliary function defined in (4). *Then there exists at least one solution $x(t)$ of the periodic problem* (18) *such that for all $t \in [0, T]$*

$$U \leq x(t) \leq L.$$

Next, we introduce an important result due to R. Ortega and N. Dancer [3], that relates the Lower and Upper Solutions Method and the instability.

Proposition 1 ([3], Proposition 3.1 and its remark) *Assume that* (18) *has strict lower and upper solutions, L and U, respectively, satisfying $L(t) < U(t)$ for all $t \in \mathbb{R}$. In addition, assume that f satisfies the Nagumo condition (for a definition see [4], chapter 1, section 4) and that the number of T-periodic solutions satisfying $L(t) < x(t) < U(t)$ for all $t \in \mathbb{R}$, is finite. Then at least one of them is unstable.*

A necessary Lemma in order to get multiplicity results is given in this section.

Lemma 1 ([7]) *Consider equation* (17) *and assume that f is a function in $\bar{D} = \mathbb{R}\times]\mathrm{x}_1, \mathrm{x}_2[\times \mathbb{R}$, with second partial derivatives continuous in $\bar{D}$. If additionally f depends linearly on v such that $f(t, x, v) = bv + g(t, x)$ where*

$$\partial_x g(t, x) < \left(\frac{\pi}{T}\right)^2 + \frac{b^2}{4} \quad \text{and} \quad \partial_x^2 g(t, x) < 0,$$

on $D = \mathbb{R} \times]\mathrm{x}_1, \mathrm{x}_2[$, then

1. *T-periodic solutions of* (17) *are ordered for all $t \in \mathbb{R}$.*
2. *Equation* (17) *has at most two T-periodic solutions in $]\mathrm{x}_1, \mathrm{x}_2[$.*

Appendix B: Some auxiliary results

Next we present some auxiliary results about linear second order differential equations with periodic coefficients.

Proposition 2 (Liapounoff-Zukovskii, [19]) *Let $a(t) \in C(\mathbb{R}/\mathrm{T}\mathbb{Z})$ such that $0 < a(t) \leq \left(\frac{\pi}{T}\right)^2$ for all $t \in \mathbb{R}$, with strict inequality on a set of positive measures in $[0, T]$. Then Hill's equation*

$$\ddot{y} + a(t)y = 0,$$

is elliptic.

Consider the second order differential equation with damping

$$\ddot{y} + b\dot{y} + a(t)y = 0, \tag{19}$$

where $a(t) \in C(\mathbb{R}/\mathrm{T}\mathbb{Z})$ and $b > 0$.

Lemma 2 ([14]) *Consider the change of variable $z = \mathrm{e}^{\frac{1}{2}bt}y$, where $a(t) \in C(\mathbb{R}/\mathrm{T}\mathbb{Z})$ and $b > 0$. Then*

1. *Equation* (19) *is transformed into standard Hill's equation:*

   $$\ddot{z} + Q(t)z = 0, \tag{20}$$

   where $Q(t) = a(t) - \frac{b^2}{4}$. Moreover, if ρ_1, ρ_2 are the characteristic multipliers of (20) *and λ_1, λ_2 are the characteristic multipliers of* (19) *then*

   $$\lambda_1 = \mathrm{e}^{-\frac{1}{2}bT}\rho_1 \quad \text{and} \quad \lambda_2 = \mathrm{e}^{-\frac{1}{2}bT}\rho_2.$$

2. *If Hill's equation* (20) *is elliptic then the characteristic multipliers of* (19) *satisfy*

   $$|\lambda_1| < 1 \quad \text{and} \quad |\lambda_2| < 1.$$

Lemma 3 *Consider* (19) *and assume that $a(t) < 0$ for all $t \in \mathbb{R}$. Then* (19) *can not admit non-trivial T-periodic solutions.*

References

1. Ai, S., Pelesko, J.A.: Dynamics of a canonical electrostatic mems/nems system. Journal of Dynamics and Differential Equations **20**(3), 609–641 (2008). doi:10.1007/s10884-007-9094-x
2. Anjum, N., He, J.H.: Nonlinear dynamic analysis of vibratory behavior of a graphene nano/microelectromechanical system. Mathematical Methods in the Applied Sciences (2020). doi:10.1002/mma.6699
3. Dancer, E.N., Ortega, R.: The index of lyapunov stable fixed points in two dimensions. Journal of Dynamics and Differential Equations **6**(4), 631–637 (1994). doi:10.1007/bf02218851
4. De Coster, C., Habets, P.: Two-point boundary value problems: lower and upper solutions, vol. 205. Elsevier (2006). doi:10.1016/s0076-5392(06)x8055-4
5. Gardner, J.W., Varadan, V.K., Awadelkarim, O.O.: Microsensors, MEMS, and smart devices, vol. 1. Wiley New York (2001). doi:10.1002/9780470846087
6. Gómez, H., Ram, M.K., Alvi, F., Villalba, P., Stefanakos, E.L., Kumar, A.: Graphene-conducting polymer nanocomposite as novel electrode for supercapacitors. Journal of Power Sources **196**(8), 4102–4108 (2011). doi:10.1016/j.jpowsour.2010.11.002
7. Gutiérrez, A., Torres, P.J.: Nonautonomous saddle-node bifurcation in a canonical electrostatic mems. International Journal of Bifurcation and Chaos **23**(05), 1350088 (2013). doi:10.1142/s0218127413500880
8. Hazim, H., Wei, D., Elgindi, M., Soukiassian, Y.: A lumped-parameter model for nonlinear waves in graphene. World Journal of Engineering and Technology **03**(02), 57–69 (2015). doi:10.4236/wjet.2015.32006
9. Khan, Z.H., Kermany, A.R., Öchsner, A., Iacopi, F.: Mechanical and electromechanical properties of graphene and their potential application in MEMS. Journal of Physics D: Applied Physics **50**(5), 053003 (2017). doi:10.1088/1361-6463/50/5/053003
10. Krauskopf, B., Osinga, H.M., Galán-Vioque, J. (eds.): Numerical Continuation Methods for Dynamical Systems. Springer Netherlands (2007). doi:10.1007/978-1-4020-6356-5
11. Le, L.T., Ervin, M.H., Qiu, H., Fuchs, B.E., Lee, W.Y.: Graphene supercapacitor electrodes fabricated by inkjet printing and thermal reduction of graphene oxide. Electrochemistry Communications **13**(4), 355–358 (2011). doi:10.1016/j.elecom.2011.01.023
12. Lee, C., Wei, X., Kysar, J.W., Hone, J.: Measurement of the elastic properties and intrinsic strength of monolayer graphene. Science **321**(5887), 385–388 (2008). doi:10.1126/science.1157996
13. Li, Y.: Reversible wrinkles of monolayer graphene on a polymer substrate: toward stretchable and flexible electronics. Soft Matter **12**(13), 3202–3213 (2016). doi:10.1039/c6sm00108d
14. Llibre, J., Núñez, D.E., Rivera, A.: Periodic solutions of the nathanson's and the comb-drive models. International Journal of Non-Linear Mechanics **104**, 109–115 (2018). doi:10.1016/j.ijnonlinmec.2018.05.009
15. Martin-Olmos, C., Rasool, H.I., Weiller, B.H., Gimzewski, J.K.: Graphene MEMS: AFM probe performance improvement. ACS Nano **7**(5), 4164–4170 (2013). doi:10.1021/nn400557b
16. Núñez, D.E., Perdomo, O., Rivera, A.: On the stability of periodic solutions with defined sign in mems via lower and upper solutions. Nonlinear Analysis: Real World Applications **46**, 195–218 (2019). doi:10.1016/j.nonrwa.2018.09.010
17. Skrzypacz, P., Kadyrov, S., Nurakhmetov, D., Wei, D.: Analysis of dynamic pull-in voltage of a graphene mems model. Nonlinear Analysis: Real World Applications **45**, 581–589 (2019). doi:10.1016/j.nonrwa.2018.07.025
18. Skrzypacz, P., Omarov, D., Nurakhmetov, D., Wei, D.: On the application of sturm's theorem to analysis of dynamic pull-in for a graphene-based mems model. Applied and computational mechanics **12** (2018). doi:10.24132/acm.2018.413
19. Staržinskiĭ, V.M.: Survey of works on conditions of stability of the trivial solution of a system of linear differential equations with periodic coefficients (1955). doi:10.1090/trans2/001/09
20. Tian, H., Ren, T.L., Xie, D., Wang, Y.F., Zhou, C.J., Feng, T.T., Fu, D., Yang, Y., Peng, P.G., Wang, L.G., Liu, L.T.: Graphene-on-paper sound source devices. ACS Nano **5**(6), 4878–4885 (2011). doi:10.1021/nn2009535
21. Wei, D., Kadyrov, S., Kazbek, Z.: Periodic solutions of a graphene based model in micro-electro-mechanical pull-in device. Applied and Computational Mechanics **11**(1), 81–90 (2017). doi:10.24132/acm.2017.322
22. Younis, M.I.: MEMS linear and nonlinear statics and dynamics, vol. 20. Springer Science & Business Media (2011). doi:10.1007/978-1-4419-6020-7
23. Zang, X., Zhou, Q., Chang, J., Liu, Y., Lin, L.: Graphene and carbon nanotube (CNT) in MEMS/NEMS applications. Microelectronic Engineering **132**, 192–206 (2015). doi:10.1016/j.mee.2014.10.023
24. Zhang, Y., Gu, Y.: Mechanical properties of graphene: Effects of layer number, temperature and isotope. Computational Materials Science **71**, 197–200 (2013). doi:10.1016/j.commatsci.2013.01.032